

Accepted Manuscript

Title: Acetalization of acetone with glycerol catalyzed by niobium-aluminum mixed oxides synthesized by a sol-gel process

Author: Raphael Rodrigues Dalmo Mandelli Norberto S. Gonçalves Paolo P. Pescarmona Wagner A. Carvalho



PII: S1381-1169(16)30036-X
DOI: <http://dx.doi.org/doi:10.1016/j.molcata.2016.02.002>
Reference: MOLCAA 9767

To appear in: *Journal of Molecular Catalysis A: Chemical*

Received date: 29-9-2015
Revised date: 30-1-2016
Accepted date: 1-2-2016

Please cite this article as: Raphael Rodrigues, Dalmo Mandelli, Norberto S. Gonçalves, Paolo P. Pescarmona, Wagner A. Carvalho, Acetalization of acetone with glycerol catalyzed by niobium-aluminum mixed oxides synthesized by a sol-gel process, Journal of Molecular Catalysis A: Chemical <http://dx.doi.org/10.1016/j.molcata.2016.02.002>

This is a PDF file of an unedited manuscript that has been accepted for publication. As a service to our customers we are providing this early version of the manuscript. The manuscript will undergo copyediting, typesetting, and review of the resulting proof before it is published in its final form. Please note that during the production process errors may be discovered which could affect the content, and all legal disclaimers that apply to the journal pertain.

Acetalization of acetone with glycerol catalyzed by niobium-aluminum mixed oxides synthesized by a sol-gel process

Raphael Rodrigues^{a,c*}, Dalmo Mandelli^a, Norberto S.Gonçalves^b, Paolo P. Pescarmona^{c,d}, Wagner A. Carvalho^a

^aCentre of Natural and Human Sciences, Federal University of ABC, 166 Santa Adélia Street, Bangu, Santo André, SP, 09210-170, Brazil.

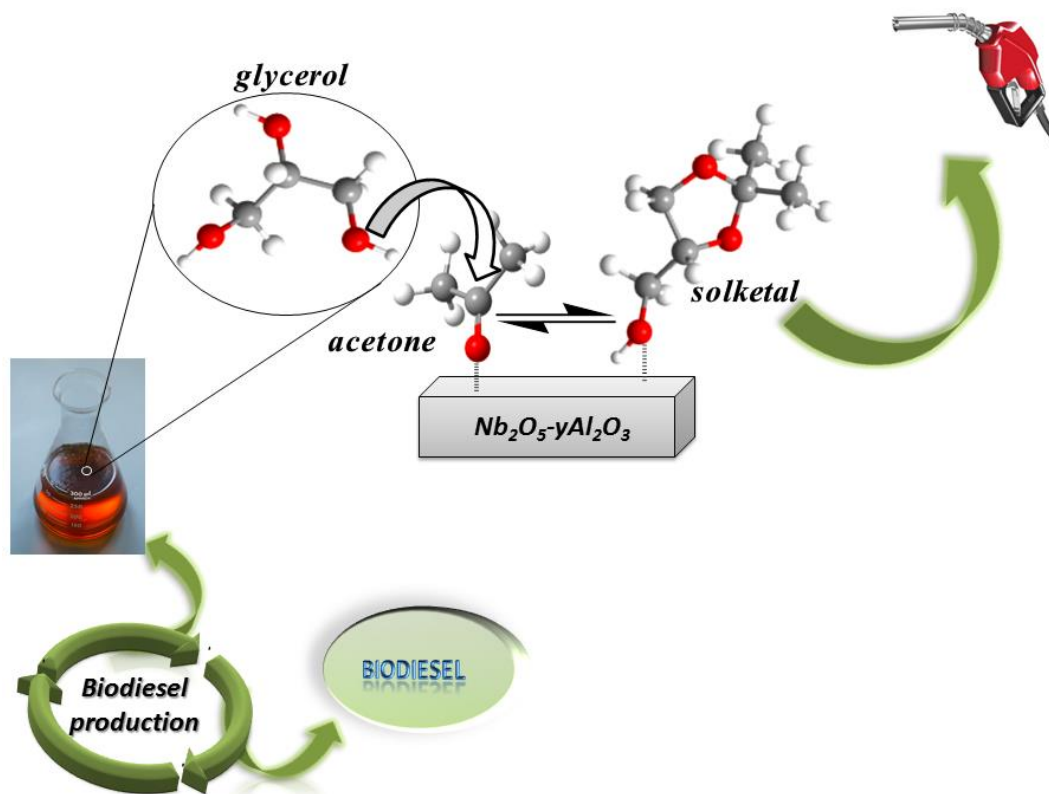
^bFederal University of São Paulo, 275 Prof. Artur Riedel Street, Jd. Eldorado, Diadema, SP, 09972-270.

^cCentre for Surface Chemistry and Catalysis, KU Leuven, Kasteelpark Arenberg 23, 3001 Heverlee, Belgium.

^dChemical Engineering Department, University of Groningen, Nijenborgh 4, 9747 AG, Groningen, The Netherlands.

*Corresponding author. Tel.: +55 (11) 4996-8386; Fax: +55 (11) 4996-8386. E-mail address: rapharod@globo.com

Graphical Abstract



Highlights

- Niobium-aluminum-based mixed oxide highly active in the acetalization of acetone with glycerol and selective towards solketal.
- Set of catalysts synthesized by a sol-gel process using high-throughput techniques to optimize the catalytic features of the solids.
- Nb-O-Al bonds are crucial to the persistence of niobic acid-like structure of the NbO_x species in these compositions even after thermal treatment at 823 K.
- Hydrophilicity of the catalysts surface plays an important role in the catalytic performance of the materials, beside the acid sites.

ABSTRACT

Niobium-aluminum-based catalysts were synthesized by a sol-gel process and successfully applied to the reaction of acetalization of acetone with glycerol yielding 2,2-dimethyl-1,3-dioxolane-4-methanol (solketal) and 2,2-dimethyl-1,3-dioxan-5-ol.

The synthesis procedure was developed using high-throughput techniques and the materials prepared with molar ratio 1 Metal (1Nb:xAl) : 100H₂O : 1.5NH₄OH (in which $x = 1, 0.6, 0.3, 0.1$ and 0.05) were selected to be further investigated. The obtained series of mixed oxides displayed high catalytic activity reaching glycerol conversion up to 84%, with 98% of selectivity towards solketal. The physicochemical properties of the investigated catalysts were characterized by N₂-adsorption/desorption, thermal analysis, X-rays diffraction, FTIR and Raman spectroscopy, and by adsorption of pyridine monitored by FT-IR spectroscopy and TGA. The catalysts are truly heterogeneous and can be reused in consecutive runs without loss of activity.

Keywords: Niobium; aluminum; acetalization; solketal; glycerol.

1. Introduction

The non-renewable nature of fossil fuel reserves combined with the increasing demand for energy has prompted humanity to look for alternative and more sustainable types of fuels. In recent years, biofuels have been developed as a promising substitute for the petroleum-based diesel [1]. However, the established biodiesel production process generates ca. 10 % of glycerol as by-product, which would represent an economic drawback to the process viability unless a valuable application is found for the crude glycerol [2]. In this context, the conversion of glycerol into added-value products has been widely studied and several viable synthetic routes have been considered, such as hydrogenolysis [3], oxidation [4], carbonatation [5], etherification [6], esterification [7] and acetalization with either aldehydes or ketones [8-11]. The acetalization of acetone with glycerol can produce two branched oxygen-containing compounds. The main product is generally solketal (2,2-dimethyl-1,3-dioxolane-4-methanol), which has potential to be directly applied as solvent, low temperature heat-transfer fluid, surfactant and fuel additive [12-13]. The reaction can also yield the six-membered-ring product (6MR), 2,2-dimethyl-1,3-dioxan-5-ol (Scheme 1) [14].

Scheme 1: Acetalization of acetone with glycerol.

Conventionally, the condensation of glycerol with either aldehydes or ketones is carried out in a homogeneous Brønsted acid catalytic system [15]. However, recently several approaches have been reported detailing the production of acetals and/or ketals via acetalization reactions by heterogeneous catalytic processes. These studies were stimulated by the economic and environmental advantages inherent to heterogeneous catalysis. Solid acids such as Amberlyst-type resins [16], zeolites [9, 15, 17], mesoporous metal-substituted silicates [10, 18], mixed oxides [19], niobic acid [20], sulfated zirconia [21] and functionalized activated carbons [22, 23] have been successfully applied as catalysts for the acetalization of acetone with glycerol.

Recently, niobium pentoxide (Nb_2O_5) has gained much attention due to its remarkable properties, both as support and as catalyst. Niobium-oxide-based materials own a set of attractive catalytic features including redox properties and acidity, and they have been pointed out as active catalysts in several acid-catalyzed reactions [24]. The catalytic properties of $\text{Nb}_2\text{O}_5 \cdot n\text{H}_2\text{O}$, i.e. niobic acid, including acidity, are directly related to its structure. Hydrated niobium oxide compounds predominantly contain octahedrally-coordinated NbO_6 units with different extents of distortion due to corner- or edge-shared NbO_6 polyhedra and NbO_4 tetrahedra [25, 26]. The incidence of the highly polarized $\text{Nb}=\text{O}$ double bond in NbO_4 , contributes to the generation of Lewis acidity, whereas the slightly distorted NbO_6 , NbO_7 and NbO_8 are characterized by $\text{Nb}-\text{O}-\text{Nb}$ single bonds and, due to the highly polarized $\text{Nb}-\text{O}$ bonds in these distorted polyhedral, some of the surface OH groups function as Brønsted acid sites [27, 28]. It is well documented that full transition of amorphous hydrated Nb_2O_5 to a crystalline form, which typically takes place upon thermal treatment at high temperatures (above 973 K), is followed by a decrease of its acidic properties [27]. In this direction, Jenh and Wachs [29] first detailed the role of niobia supported over several high surface area metal oxides (MgO , TiO_2 , ZrO_2 , SiO_2 and Al_2O_3) and pointed out the effect of the support nature over the activity of the solids. Lewis acid sites were detected in all supported niobia, whereas Brønsted acid sites were observed only in $\text{Nb}_2\text{O}_5/\text{Al}_2\text{O}_3$ and $\text{Nb}_2\text{O}_5/\text{SiO}_2$. More specifically, the bridge $\text{Nb}-\text{OH}-\text{Al}$ species formed through the interaction of the NbO_x species with the hydroxyl groups present on the surface of alumina have been identified as Brønsted acid centers. In these materials, the loading of niobia is limited to the monolayer coverage [29, 30]. Based on these specific properties, $\text{Nb}_2\text{O}_5/\text{Al}_2\text{O}_3$ has been widely applied in several acid-catalyzed reactions such as

Friedel-Crafts alkylation [31], dealkylation of cumene [32] and methanol oxidation [29].

The possibility of extending the synergy between Nb and Al throughout the framework of the mixed oxide and its contribution to the catalytic activity are still poorly explored. In this work, a series of niobium and aluminum mixed oxides were synthesized by a sol-gel process in order to investigate the aforementioned synergy and relate it to the catalytic performance in the acetalization of acetone with glycerol. Several synthetic parameters were evaluated, such as hydrolysis rate, pH and Nb/Al molar ratio, aiming at understanding their influence on the catalytic activity of the obtained materials in the studied reaction.

2 Experimental

2.1 High-throughput platform

The initial screening of the synthesis of the catalysts was performed in a high-throughput platform, equipped with a heating and stirring unit containing multiple parallel wells that can host 10 mL glass vials [33]. The synthesis mixtures were prepared by dispensing the desired amounts of the solutions of aluminum sec-butoxide in sec-butanol and niobium chloride in ethanol, which were previously prepared under N₂ atmosphere in a concentration of 0.46M and 0.30M, respectively.

2.2 Synthesis of the catalysts

The standard sol-gel synthesis procedure consisted in adding a desired amount of a solution of each precursor into a 10 ml vial, followed by stirring of the mixture for 3 h. Afterwards, both water and a base (25% NH₄OH solution from Nuclear) or an acid (65% HNO₃ solution from Vetec) were added dropwise into the synthesis vial and the system was kept under stirring for further 60 min. The vial was closed and the sample aged in an oven for 24 h at 353 K. Each composition was centrifuged in order to remove the liquid phase. The obtained solids were dried in an oven at 353 K for 48 h (to achieve complete removal of the solvents) and calcined at 823 K under 100 cm³ min⁻¹ flow of air for 5 h (heating rate of 3 K min⁻¹ under 100 cm³ min⁻¹ flow of N₂). The relative amounts that were employed are: water/metal = 100, 50, 25 and 10, NH₄OH/metal = 1.5, 0.7 and 0.3, HNO₃/metal = 2, 1, 0.5 and 0 and Al/Nb= 10, 5, 1, 0.6, 0.3, 0.1, 0.05.

2.3 Characterization

The textural properties of the solids were determined by N₂ adsorption/desorption measurements on an Autosorb 1-MP device (Quantachrome Instruments). The samples were pre-treated at 473 K under vacuum for 3 h and the analysis was carried out at 77 K. The surface area, pore (void) volume and pore (void) size distribution were calculated by means of the Brunauer–Emmett–Teller (BET) equation [34] and of the density functional theory (DFT) [35]. Powder X-ray diffraction patterns (XRD) were measured on a Bruker D8 Advance diffractometer using a Cu K α radiation (1.542 Å) with a high resolution Lynxeye detector. Each sample was scanned in a 2 θ range of 20–60° with step size of 0.02°/s. Fourier-transform infrared spectroscopy (FTIR) analysis using a Varian 3100 FT-IR spectrometer were performed mixing the dried sample with potassium bromide (KBr) in a 1:50 weight ratio. This mixture was ground into a fine powder, dried at 373 K for 24 h, and used to produce thin, flat pellets by means of a manual equipment. The spectra were acquired at room temperature by accumulating 128 scans at 4cm⁻¹ resolution in the range of 400–3500 cm⁻¹. Raman spectra were recorded in a Raman Renishaw microscope (Model InVia) with exciting radiation at 830 nm (laser diode) in a range of 200–1200 cm⁻¹ with suppression of spikes caused by cosmic rays. Before measuring each spectrum, the sample was compacted in a glass lamina, in order to have a smooth surface, and focused in an optical microscope. In order to estimate hydrophilicity degree of the catalysts, thermogravimetric analysis (TGA) was performed using a Q500 TGA device (TA Instruments) under N₂ atmosphere (gas flow of 50 cm³ min⁻¹) at a heating rate of 10 K min⁻¹ in the range of 300–1000 K. Prior to TGA analysis, the samples were equilibrated in the open ambient environment for 48 h at 298 K (humidity of 30–40%).

The number of acid sites was determined based on the methodology proposed by Ghesti *et al.*[36]. The samples (~25 mg) were placed in a glass reactor and heated up to 473 K under vacuum for 90 min, in order to remove physisorbed molecules, cooled down to 373 K and subjected to a flow of pyridine in N₂(100 cm³ min⁻¹) for 20 min. The saturated samples were heated to 423 K and the temperature was held for 60 min under reduced pressure, in order to remove the excess of probe molecule. The same procedure was followed, skipping the pyridine adsorption step, in order to obtain a blank. Both saturated and non-saturated samples were subjected to a thermogravimetric analysis in a Q500 TGA device from TA Instruments. The measurements were carried out under N₂

(50 cm³ min⁻¹) at 10 K min⁻¹ from 298 K to 1073 K and the number of acid sites was calculated (Eq. 1).

$$n_{py} = \frac{\{[M_{py}/M_{py423}] - [M_{1073}/M_{423}]\}}{MM_{py}} \quad (1)$$

where:

M_{py} : Mass of desorbed pyridine = $M_{py423} - M_{py1073}$

M_{py423} : Mass of saturated sample at 423 K

M_{1073} : Mass of physisorbed molecules of the non-saturated sample (blank) = $M_{423} - M_{1073}$

M_{423} : Mass of non-saturated sample (blank) at 423 K

MM_{py} = molecular mass of pyridine, 79.101 g mol⁻¹

Furthermore, the population of Lewis and Brønsted acid sites of the materials was estimated by Fourier-transform infrared spectroscopy analysis of adsorbed pyridine at 423 K. The samples were dried at 473 K and the reference spectra were recorded. Adsorption of pyridine on the previously dried sample took place in a glass reactor at 373 K under a constant flow of a mixture of pyridine and N₂ (100 cm³ min⁻¹) for 20 min and then submitted to a thermal treatment at 423 K for 60 min. Afterwards, approximately 15 mg of each sample was placed in a self-supporting disk of 7 mm diameter and the infrared spectra were obtained using a Varian 3100 FT-IR spectrometer (512 scans and 4cm⁻¹ resolution). The number of acid sites was determined from the integral of the bands at 1445 cm⁻¹ (Lewis acid sites) and at 1540 cm⁻¹ (Brønsted acid sites), using the molar extinction coefficients previously reported by Tamura *et al.* [37].

2.4 Catalytic tests

The acetalization of acetone with glycerol was carried out in 10 ml capped glass vials under vigorous stirring (600rpm) at different temperatures (room temperature, 323 K or 353 K). In a typical catalytic test, 0.921 g (0.01 mol) of highly purified glycerol (99%), a selected amount of acetone [i.e. 0.581 g (0.01 mol), 1.162 g (0.02 mol) or

2.324 g (0.04 mol)] and 0.132 g (0.0015 mol) of 1,4-dioxane, used as the GC internal standard, were weighed in a 10 mL glass vial containing 25 mg of the catalyst. The mixture was stirred for 6 h at the selected temperature. The reaction products were analyzed by gas chromatography with flame ionization detector (GC-FID) using an Agilent 7890A device, equipped with a DB-WAX capillary column.

3. Results and discussion

In order to establish the best synthetic conditions adopted to prepare a set of niobium-aluminum mixed oxides, several parameter of the sol-gel process were evaluated using a high-throughput platform. Both catalytic activity and reproducibility indicated that the best conditions to synthesize a niobium-aluminum mixed oxide with promising performance in the reaction of acetalization of acetone with glycerol imply the use of a highly basic medium with an excess of water. The catalysts containing high amount of aluminum oxide (Al/Nb molar ratio of 5 and 10) as well as all the solids synthesized in acid medium were inactive (glycerol conversion lower than 5%). Based on this preliminary high-throughput screening, a synthesis protocol was selected to synthesize the catalysts to be further investigated on the acetalization of acetone with glycerol. This protocol is characterized by the following molar ratio: 1Metal (1Nb: x Al) : 100H₂O : 1.5NH₄OH (in which $x = 1, 0.6, 0.3, 0.1$ and 0.05).

3.1 Characterization of the catalysts

The XRD patterns of the Nb₂O₅- y Al₂O₃ catalysts calcined at 823 K are presented in Figure 1. The diffraction peaks of pure Nb₂O₅, observed at $2\theta = 22.39^\circ, 28.40^\circ, 36.72^\circ, 46.10^\circ, 50.68^\circ$ e 55.23° , can be indexed to the orthorhombic (T) phase of niobium pentoxide [27, 38]. On the other hand, the amorphous state is prevailing in both 1Nb:1Al and 1Nb:0.6Al, since the presence of bulk Nb₂O₅ is negligible for these compositions (and also in niobic acid, *i.e.* the hydrated oxide Nb₂O₅. n H₂O). Wachs *et al.* [39] claimed that the dispersion of niobia on γ -alumina takes place through the interactions of NbO _{x} with the hydroxyl groups present on γ -Al₂O₃ surface up to the monolayer coverage (about 19% (w/w)). In this work, niobium oxide persisted as an amorphous phase up to remarkable higher load of NbO _{x} in the material. This suggests the extensive presence of Nb-O-Al bonds within the oxides prepared with 1Nb:1Al and 1Nb:0.6Al. Low intensity reflection peaks of the T-Nb₂O₅ crystalline phase are also observed in 1Nb:0.3Al, 1Nb:0.1 and 1Nb:0.05Al and the presence of this crystalline

phase is due to the high load of Nb in the material, but the aforementioned Nb-O-Al bonds are expected to be still present in significant amounts, since the full transition to the orthorhombic phase was not observed in any of the niobium-aluminum mixed oxides. In the case of 1Nb:0.1Al and 1Nb:0.05Al, diffraction peaks referred to crystalline AlNbO_4 were also observed ($2\theta=23.4^\circ$, 24.8° , 31.7° , 43.8° and 47.1°) [31].

Figure 1: XRD patterns of Niobic acid, 1Nb:1Al, 1Nb:0.6Al, 1Nb:0.3Al, 1Nb:0.1Al, 1Nb:0.05Al and Nb_2O_5 .

FTIR spectra of the niobium containing materials are presented in Figure 2. The broad band in the range of $550\text{-}630\text{ cm}^{-1}$ as well as the shoulder-like band at around 900 cm^{-1} have been assigned to Nb-O and Nb=O stretching modes, respectively. The latter signal is more defined in 1Nb:0.3Al, 1Nb:0.1Al, 1Nb:0.05Al and Nb_2O_5 , and is associated to the remarkable concentration of highly distorted niobium oxide species containing Nb=O bonds in the crystalline phase [30, 40], in agreement with the XRD data presented in Figure 1. Accordingly, the band at around 900 cm^{-1} has low intensity in the spectra of the amorphous 1Nb:1Al, 1Nb:0.6Al and niobic acid samples.

Moreover, the vibration bands at around ca. 3420 cm^{-1} and 1610 cm^{-1} are associated to the OH stretching and bending modes of physisorbed water, respectively, and are more pronounced in the catalysts with higher hydrophilicity [26].

Analysis by Raman spectroscopy showed characteristic bands at around 660 cm^{-1} and at 990 cm^{-1} (Figures 3a and 3b). The signal at 660 cm^{-1} has been assigned to the symmetric stretching mode of the slightly distorted NbO_6 , NbO_7 and NbO_8 polyhedra, which are present in both amorphous and crystalline niobia. The band at 990 cm^{-1} has been assigned to the symmetric stretching mode of Nb=O, which is more pronounced in crystalline Nb_2O_5 [25, 29]. The Raman spectra of 1Nb:1Al and 1Nb:0.6Al are remarkably similar to the Raman profile observed for the amorphous niobic acid, $\text{Nb}_2\text{O}_5 \cdot n\text{H}_2\text{O}$ (Figure 3a), indicating the persistence of a niobic acid-like structure of the NbO_x species in these compositions even after thermal treatment at 823 K, in full agreement with FTIR and XRD data. In the case of 1Nb:0.3Al, the incipient presence of the T- Nb_2O_5 crystalline phase can be recognized by the slightly pronounced bands present in the low wave number region ($200\text{-}350\text{ cm}^{-1}$), which are characteristic of the bending modes of the Nb-O-Nb bonds, typically observed in T- Nb_2O_5 [25] (Figure 3b). However, the characteristic band at 990 cm^{-1} was not detected, likely due to

the low concentration of Nb=O sites in this composition. For 1Nb:0.1Al and 1Nb:0.05Al, the presence of the T-Nb₂O₅ phase becomes clearer, as evidenced by the Raman bands at around 260, 660 and 990 cm⁻¹. Nevertheless, the presence of AlNbO₄ (as suggested by XRD) cannot be disregarded since these compounds possess a highly distorted octahedral NbO_x structure with Raman bands in the high wave number region (850-1000 cm⁻¹) and the bands in the region of 200-300 cm⁻¹ assigned to the associated bending mode might be also related to this crystalline phase [25, 31].

Figure 2: FTIR spectra of 1Nb:1Al, 1Nb:0.6Al, 1Nb:0.3Al, 1Nb:0.1Al, 1Nb:0.05Al, Niobic acid; Nb₂O₅.

Figure 3: Raman spectra of (a) 1Nb:1Al, 1Nb:0.6Al and Niobic acid; (b) 1Nb:0.3Al, 1Nb:0.1Al, 1Nb:0.05Al and Nb₂O₅.

The acid properties of the catalysts were studied by thermal desorption of pyridine [36], which was monitored both by FT-IR spectroscopy and by TGA. The results with the two techniques show the same trends (Table 1). These data indicate a decreasing number of acid sites with increasing content of Nb. The bands at 1445 cm⁻¹ and 1540 cm⁻¹ in the FT-IR spectra of chemisorbed pyridine over γ -Al₂O₃ and 1Nb:*x*Al at 423 K were used to quantify Lewis and Brønsted acid sites, respectively (Figure 4). As expected, under the analysis conditions, pure γ -Al₂O₃ presented only Lewis acid sites (0.42 mol kg⁻¹), which is in agreement with previous reports [28]. In the case of the 1Nb:*x*Al oxides, most of the acid sites present on the surface are of Lewis type. However, Brønsted acid sites were also detected in 1Nb:1Al, 1Nb:0.6Al and 1Nb:0.3Al (Table 1). It is expected that the generation of weak Brønsted acid sites is related to the bridged Nb-OH-Al but the contribution of Nb-OH-Nb species should be also relevant [30, 41]. On the other hand, Lewis acidity could stem both from the polymeric amorphous NbO_x in niobic acid-like form, as from Al₂O₃ domains. It should be noted that the ratio between Lewis and Brønsted acid sites was not strongly affected by the Nb:Al ratio (for *x* = 1, 0.6 and 0.3, see Table 1). For the materials with a lower Al content (1Nb:0.1Al and 1Nb:0.05Al), the low total concentration of acid sites prevented the quantification of the Lewis and Brønsted acid species.

Table 1: Textural properties and acidity of 1Nb:1Al, 1Nb:0.6Al, 1Nb:0.3Al, 1Nb:0.1Al and 1Nb:0.05Al

Figure 4: Infrared spectrum of chemisorbed pyridine over γ -Al₂O₃, 1Nb:1Al, 1Nb:0.6Al and 1Nb:0.3Al at 423 K

Both surface area and pore volume distribution were calculated from the nitrogen physisorption isotherm obtained by N₂adsorption/desorption analysis. Based on the isotherms presented in Figure 5a, it is noteworthy that the samples containing higher amount of aluminum oxide (1Nb:1Al and 1Nb:0.6Al) display a Type IV isotherm, with an H3 hysteresis loop, which is observed with aggregates of plate-like particles giving rise to slit-shaped mesopores or interparticle voids in the mesoscale [42]. Since no structure directing agent was used in the synthesis of the materials, the observed porosity is attributed to interparticle voids. On the other hand, the N₂ isotherms of 1Nb:0.3Al, 1Nb:0.1Al and 1Nb:0.05Al are classified as Type II, which is expected for non-porous materials, and a slightly pronounced H3 hysteresis loop can be observed in the isotherms [42] (Figure 5b). The pore size distribution of 1Nb:1Al and 1Nb:0.6Al, (Figure 6a), is mainly in the mesoscale region below 20 nm whereas that of the materials with lower Al content is very broad and with low dV/dD values (Figure 6b). The surface area and the pore volume decrease significantly with increasing Nb content in the catalysts (Table 1).

Figure 5: N₂ adsorption/desorption isotherms of (a) 1Nb:1Al, 1Nb:0.6Al and (b) 1Nb:0.3Al, 1Nb:0.1Al, 1Nb:0.05Al.

Figure 6: Pore distribution of (a) 1Nb:1Al, 1Nb:0.6Al and (b) 1Nb:0.3Al, 1Nb:0.1Al, 1Nb:0.05Al.

The calcination step in the synthesis of the catalysts was thoroughly investigated by thermogravimetric analysis (TG-DTA, see Figures 7 and 8). Thermal events observed at temperatures below 393 K are ascribed to the loss of moisture and of remaining solvents used during the sol-gel synthesis procedures. The next events have an endothermic nature and can be assigned to the loss of hydroxyl groups present on the surface of the mixed oxides and on bulk Nb₂O₅ as a consequence of the condensation of oxi-hydroxy NbO₂(OH) species [43]. The exothermic event at approximately 830 K in 1Nb:0.3Al, 1Nb:0.1Al and 1Nb:0.05Al is related to the first crystalline transition of the niobium oxide, and the weight loss observed at this temperature might be associated

with a change in the composition. Accordingly, no thermal event at about 830 K was observed for the amorphous materials (1Nb:1Al and 1Nb:0.6Al).

Figure 7: Thermogravimetric analysis of 1Nb:1Al, 1Nb:0.6Al, 1Nb:0.3Al, 1Nb:0.1Al and 1Nb:0.05Al.

Figure 8: Differential thermal analysis of 1Nb:1Al, 1Nb:0.6Al, 1Nb:0.3Al, 1Nb:0.1Al and 1Nb:0.05Al.

3.2 Catalytic tests

The conversion of glycerol to solketal via acetalization of acetone takes place over acid sites [44], but in the case of heterogeneous catalysts the textural and surface properties also play an important role [10]. Therefore, the synthesized Nb-Al-based acid catalysts herein presented were investigated in the acetalization of acetone with glycerol, and the role of the structural properties and acidity in the catalytic performance of these mixed oxides was evaluated. First, the relationship between the glycerol conversion and the molar ratio of glycerol to acetone was studied (Figure 9a). The experiments were carried out at 323 K for 6 h. As expected, the conversion of glycerol remarkably increases with the relative amount of acetone in the reaction medium [10,45], reaching 84% of substrate conversion with acetone:glycerol = 4:1 over 1Nb:0.05Al. Fan *et al.*[45] applied successfully a Ti-Si-based catalyst in the acetalization of acetone with glycerol reaching up to 86% of glycerol conversion with 90% of selectivity to solketal. Nandan *et al.* [46] explored the viability of a series of sulfonated carbon-silica-meso composite materials as catalyst in the conversion of glycerol to solketal via acetalization with acetone and achieved glycerol conversion as high as 82% with selectivity to the main product of 99%. Based on the typical acetalization reaction mechanism of ketal formation over Brønsted acid sites [9], it is expected that the excess acetone shifts the equilibrium towards the products and facilitates its chemisorption over the active centers of the catalysts, which is the first step of the catalytic cycle, justifying the rise in glycerol conversion levels. Furthermore, the herein synthesized mixed oxides own a remarkable population of surface Lewis acid sites, which may contribute in catalyzing the acetalization of acetone with glycerol [10]. However, it should be kept in mind that these Lewis acid sites may convert into Brønsted ones by reacting with the water formed during the acetalization reaction [47].

The presence of Lewis acid sites at the surface of the Nb-Al mixed oxides can also play a role in coordinating glycerol, similarly to what has been reported on niobia [47].

The formation of the five-membered-ring of solketal involves the formation of a bond between the carbonyl oxygen atom of acetone and the β -carbon of the glycerol, accompanied by dehydration [10]. The less common six-membered-ring product requires the formation of a bond between the carbonyl oxygen of acetone and the primary carbon of glycerol. In agreement with previous reports [10], solketal was the major product over the Nb-Al mixed oxides (Figure 9b). For comparison, pure alumina and niobia were evaluated on the studied reaction at following conditions: glycerol:acetone molar ratio of 1:4, 2.7 wt% of catalyst and 323K, and the former catalyst showed no activity, whereas T-Nb₂O₅ gave 58% of glycerol conversion, which is in agreement with previous reports [38]. The low activity of the crystalline T-Nb₂O₅ is connected to the previously reported decrease of acidic properties upon transition from amorphous niobia to the orthorhombic T-Nb₂O₅ phase [38].

Figure 9: Effect of the variation of the glycerol to acetone ratio on the acetalization reaction (2.7 wt% of catalyst, 6 h at 323 K): (a) glycerol conversion and (b) solketal selectivity.

Experiments at different temperatures (room temperature, 323 K and 353 K) were also carried out (Table 2). Surprisingly, the catalysts with lower surface area and lower number of surface acid sites (1Nb:0.3Al, 1Nb:0.1Al and 1Nb:0.05Al) were substantially active in the reaction conducted at room temperature achieving up to 73% of glycerol conversion, while 1Nb:1Al and 1Nb:0.6Al displayed markedly worse performance under these conditions. The differences between the activity of the various catalysts was much less marked when the temperature of the process was raised to 323 K and 353 K. The best performance of 1Nb:0.3Al, 1Nb:0.1Al and 1Nb:0.05Al was reached at 323 K, whereas slightly lower conversion was observed at 353 K (Table 2). Such trend has been observed before and is attributed to the exothermic nature of the acetalization reaction, which implies lower products concentration at equilibrium upon increase of the reaction temperature [23, 48]. On the other hand, the catalytic performance of 1Nb:1Al and 1Nb:0.6Al is dependent on the temperature because at lower temperature the reaction rate over these catalysts is not sufficient to reach the equilibrium concentrations. This might seem counterintuitive, because 1Nb:1Al and 1Nb:0.6Al display the two largest populations of acid sites among the studied mixed oxides (Table

1). To understand this catalytic trend, the hydrophilicity of the materials should be considered [10]. A high hydrophilicity would prevent removal of the water formed during the acetalization from the active sites, thus favoring the reverse reaction in which the formed solketal is hydrolyzed back to glycerol and acetone. To evaluate the hydrophilicity of the catalysts, thermogravimetric analysis (TGA) was performed (Figure 10). The weight loss observed at temperatures below 523K is assigned to the desorption of water from the surface of the catalysts, which is related to the hydrophilicity of the materials. This event is much more marked in the thermogravimetric analysis of 1Nb:1Al and 1Nb:0.6Al, probably due to the high aluminum content in these materials. Combining the TGA data and the observed catalytic trends, we propose that the hydrophilicity of 1Nb:1Al and 1Nb:0.6Al plays an important role in limiting the catalytic performance of these materials.

Figure 10: Thermogravimetric analysis of the calcined 1Nb:1Al, 1Nb:0.6Al, 1Nb:0.3Al, 1Nb:0.1Al and 1Nb:0.05Al.

These results drive us to conclude that not only the presence of acid sites is required for catalyzing the acetalization reaction, but also a sufficient hydrophobicity of the catalyst surface, as that in 1Nb:0.3Al, 1Nb:0.1Al and 1Nb:0.05Al, is necessary to achieve good catalytic activity.

Table 2: Acetalization of acetone with glycerol over 1Nb:1Al, 1Nb:0.6Al, 1Nb:0.3Al, 1Nb:0.1Al and 1Nb:0.05 Al at room temperature, 323 and 353 K (glycerol : acetone molar ratio of 1:4, 2.7 wt% of catalyst, 6 h)

The activity of the catalysts as a function of time was investigated by performing a kinetic study of the acetalization of acetone with glycerol at 323 K with acetone:glycerol molar ratio of 4:1 (Figure11). The reaction catalyzed by 1Nb:0.05Al reaches equilibrium conditions after 120 min (glycerol conversion of 84%), whereas the plateau is reached at longer reaction times for the other catalysts. The difference in catalytic activity between the materials are more marked when the initial rate is considered, as can be seen by comparing the glycerol conversion in the first 20 min of reaction (Figure 11).

Figure 11: Kinetic study (solid lines) and leaching test (dashed lines) of the acetalization of acetone with glycerol catalyzed by 1Nb:1Al, 1Nb:0.6Al, 1Nb:0.3Al, 1Nb:0.1Al and 1Nb:0.05Al (glycerol:acetone molar ratio of 1:4, 2.7 wt% of catalyst, 323K).

For all the catalysts tested at 323K, the selectivity to solketal was extremely high at equilibrium conversions, but a significant amount of six-membered-ring (6MR) was observed at lower conversions, and thus particularly in the reactions catalyzed by 1Nb:1Al and 1Nb:0.6Al (Figure 12). It is noteworthy that selectivity to 6MR decreases during the reaction while the selectivity to solketal increases. The energies of the five- and six-membered-ring isomers were calculated by Mota *et al.* [49] and it was found that solketal is $1.7 \text{ kcal mol}^{-1}$ more stable than the six-membered-ring demonstrating that solketal is the thermodynamically favored product of the acetalization of acetone with glycerol. Therefore, it is expected the 6MR isomerizes to solketal throughout the reaction, explaining the observed trend for solketal selectivity.

Figure 12: Solketal and 6MR selectivity in function of time of the acetalization of glycerol with acetone catalyzed by 1Nb:1Al, 1Nb:0.6Al, 1Nb:0.3Al, 1Nb:0.1Al and 1Nb:0.05Al (glycerol:acetone molar ratio of 1:4, 2.7 wt% of catalyst, 323K).

In order to confirm the truly heterogeneous nature of the catalysts, leaching tests were carried out by removing the catalysts from the reaction medium after about 20 min allowing the liquid mixture to react in the absence of the heterogeneous catalyst for further 240 min (dashed line in Figure 11). In all evaluated systems, there was no appreciable increase in the glycerol conversion upon removing the catalyst, which indicates the lack of leaching of the active sites from the solid catalysts, as expected for a typical heterogeneous catalytic process.

Furthermore, the stability of the catalytic activity of 1Nb:1Al, 1Nb:0.3Al and 1Nb:0.1Al was evaluated in consecutive runs by separating the heterogeneous catalysts from the reaction medium after 6 h reaction time, washing the material 3 times with a polar aprotic solvent (acetonitrile) and drying the catalysts at 353 K for 24 h. In all cases, the catalytic activity remains approximately constant in the four catalytic runs (Figure 13), which indicates that acetonitrile solubilize remaining reactants and products adsorbed over the active sites avoiding any thermal treatment at high temperature to remove those species. It should be noted that a less polar aprotic solvents as acetone or a protic polar solvent as methanol were much less efficient in removing the reaction residues.

Figure 13: Recycling tests of the 1Nb:1Al at 353 K, 1Nb:0.3Al and 1Nb:0.1Al at 323K in the acetalization of glycerol with acetone (glycerol:acetone molar ratio of 1 : 4, 2.7 wt% of catalyst, 6 h).

4. Conclusions

New niobium-aluminum mixed oxides synthesized by a sol-gel process presented high catalytic activity in the acetalization of acetone with glycerol with high selectivity towards the desired product (solketal). All the prepared mixed oxides of Nb and Al display acid sites that can act as active sites for catalyzing the acetalization reaction. However, the trends in activity cannot be explained only based on the presence of acid sites and require taking into account the hydrophilicity of the catalysts surface, with the more hydrophobic materials giving the best catalytic performance. The catalysts are truly heterogeneous as no leaching of active species was observed and retained their activity in several consecutive runs.

5. Acknowledgements

This work was supported by FAPESP (Project No. 2013/21160-6), CNPq-SWB (Project No. 245705/2012-0), CNPq-FWO (CNPq-Project No.490298/2009-5, FWO-Project code: VS.025.10N, V4.520.11N) and START1 (KU Leuven, Project code: STRT1/10/035).

6. References

- [1] M.S.P. Gomes, M.S. Muylaert de Araújo, *Renew. Sust. Energ. Rev.*, 13 (2009) 2201-2204.
- [2] A. Beatriz, Y.J.K. Araujo, D.P. de Lima, *Quim. Nova*, 34 (2011) 306-319.
- [3] Z.W. Huang, F. Cui, J.J. Xue, J.L. Zuo, J. Chen, C.G. Xia, *Catal. Today*, 183 (2012) 42-51.
- [4] G.L. Brett, Q. He, C. Hammond, P.J. Miedziak, N. Dimitratos, M. Sankar, A.A. Herzing, M. Conte, J.A. Lopez-Sanchez, C.J. Kiely, D.W. Knight, S.H. Taylor, G.J. Hutchings, *Angew. Chem. Int. Ed. Engl.*, 123 (2011) 10318-10321.
- [5] N. Ezhova, I. Korosteleva, N. Kolesnichenko, A. Kuz'min, S. Khadzhiev, M. Vasil'eva, Z. Voronina, *Petroleum Chem.*, 52 (2012) 91-96.
- [6] P.A. Celdeira, M. Gonçalves, F.C.A. Figueiredo, S.M.D. Bosco, D. Mandelli, W.A. Carvalho, *Appl. Catal. A*, 478 (2014) 98-106.
- [7] S. Zhu, Y. Zhu, X. Gao, T. Mo, Y. Zhu, Y. Li, *Biores.Technol.*, 130 (2013) 45-51.
- [8] A. Behr, J. Eilting, K. Irawadi, J. Leschinski, F. Lindner, *Green Chem.*, 10 (2008) 13-30.

- [9] C.X.A. da Silva, V.L.C. Goncalves, C.J.A. Mota, *Green Chem.*, 11 (2009) 38-41.
- [10] L. Li, T.I. Koranyi, B.F. Sels, P.P. Pescarmona, *Green Chem.*, 14 (2012) 1611-1619.
- [11] B. Mallesham, P. Sudarsanam, G. Raju, B.M. Reddy, *Green Chem.*, 15 (2013) 478-489.
- [12] M. J. Climent, A. Corma and A. Velty, *Appl. Catal., A*, 263 (2004) 155–161.
- [13] M. J. Climent, A. Velty and A. Corma, *Green Chem.*, 4 (2002) 565–569.
- [14] R. Rodrigues, M. Gonçalves, D. Mandelli, P.P. Pescarmona, W.A. Carvalho, *Catal.Sci. Technol.*, 4 (2014) 2293-2301.
- [15] J. Deutsch, A. Martin, H. Lieske, *J. Catal.*, 245 (2007) 428-435.
- [16] M.R. Nanda, Z. Yuan, W. Qin, H.S. Ghaziaskar, M.-A. Poirier, C. Xu, *Fuel*, 128 (2014) 113-119.
- [17] P. Manjunathan, S.P. Maradur, A.B. Halgeri, G.V. Shanbhag, *J. Mol.Catal. A*, 396 (2015) 47-54.
- [18] L. Li, D. Cani, P.P. Pescarmona, *Inorg. Chim. Acta*, 4319 (2015) 289-296.
- [19] S. Zhang, Z. Zhao, Y. Ao, *Appl. Catal. A*, 496 (2015) 32-39.
- [20] T.E. Souza, M.F. Portilho, P.M.T.G. Souza, P.P. Souza, L.C.A. Oliveira, *ChemCatChem*, 6 (2014) 2961-2969.
- [21] P.S. Reddy, P. Sudarsanam, B. Mallesham, G. Raju, B.M. Reddy, *J. Ind. Eng. Chem.*, 17 (2011) 377-381.
- [22] M.S. Khayoon, B.H. Hameed, *Appl. Catal. A*, 464-465 (2013) 191-199.
- [23] R. Rodrigues, M. Goncalves, D. Mandelli, P.P. Pescarmona, W.A. Carvalho, *Catal.Sci. Technol.*, 4 (2014) 2293-2301.
- [24] K. Tanabe, S. Okazaki, *Appl. Catal. A*, 133 (1995) 191-218.
- [25] J.M. Jehng, I.E. Wachs, *Chem. Mater.*, 3 (1991) 100-107.
- [26] K. Nakajima, Y. Baba, R. Noma, M. Kitano, J. N. Kondo, S. Hayashi, M. Hara, *J. Am. Chem. Soc.*, 133 (2011) 4224-4227
- [27] I. Nowak, M. Ziolk, *Chem. Rev.*, 99 (1999) 3603-3624.
- [28] T. Kitano, T. Shishido, K. Teramura, T. Tanaka, *J. Phys. Chem. C.*, 116 (2012) 11615-11625.
- [29] J.-M. Jehng, I.E. Wachs, *Catal.Today*, 8 (1990) 37-55.
- [30] J. Datka, A.M. Turek, J.M. Jehng, I.E. Wachs, *J. Catal.*, 135 (1992) 186-199.
- [31] T. Shishido, T. Kitano, K. Teramura, T. Tanaka, *Top. Catal.*, 53 (2010) 672-677.

- [32] C.L.T. da Silva, V.L.L. Camorim, J.L. Zotin, M.L.R. Duarte Pereira, A.d.C. Faro Jr, *Catal. Today*, 57 (2000) 209-217.
- [33] P.P. Pescarmona, P.A. Jacobs, *Catal. Today*, 137 (2008) 52-60.
- [34] B.C. Lippens, J.H. de Boer, *J. Catal.*, 4 (1965) 319-323.
- [35] J. Olivier, W. Conklin, M. Szombathely, *Stud.Surf. Sci. Catal.*, 87 (1994) 81-89.
- [36] G.F. Ghesti, J.L. de Macedo, V.C. Parente, J.A. Dias, S.C. Dias, *Microporous Mesoporous Mater.*, 100 (2007) 27-34.
- [37] M. Tamura, K.I. Shimizu, A. Satsuma, *Appl. Catal. A: Gen.*, 433-434 (2012) 135-145.
- [38] G.S. Nair, E. Adrijanto, A. Alsalme, I.V. Kozhevnikov, D.J. Cooke, D.R. Brown, N.R. Shiju, *Catal.Sci. Technol.*, 2 (2012) 1173-1179.
- [39] I.E. Wachs, *Catal. Today*, 27 (1996) 437-455.
- [40] F. Houshang, H. Fatemeh, R. Rahmatollah, G. Ali, *J. Clust. Sci.*, 25 (2014) 651-666.
- [41] T. Kitano, T. Shishido, K. Teramura, T. Tanaka, *Catal. Today*, 226 (2014) 97-102.
- [42] K.S.W. Sing, in: *Pure Appl.Chem.*, 1985, pp. 603.
- [43] T.E. Souza, I.D. Padula, M.M.G. Teodoro, P. Chagas, J.M. Resende, P.P. Souza, L.C.A. Oliveira, *Catal.Today*, 213 (2013) 65-72.
- [44] B. Mallesham, P. Sudarsanam, G. Raju, B.M. Reddy, *Green Chem.*, 15 (2013) 478-489.
- [45] C.-N. Fan, C.-H. Xu, C.-Q. Liu, Z.-Y. Huang, J.-Y. Liu, Z.-X. Ye, *React. Kinet. Mech. Cat.*, 107 (2012) 189-202.
- [46] D. Nandan, P. Sreenivasulu, L.N. Sivakumar Konathala, M. Kumar, N. Viswanadham, *Microporous and Mesoporous Mater.*, 179 (2013) 182-190.
- [47] G. S. Foo, D. Wei, D. S. Sholl, C. Sievers, *ACS Catalysis*, 4 (2014) 3180-3192.
- [48] M.R. Nanda, Z. Yuan, W. Qin, H.S. Ghaziaskar, M.-A. Poirier, C.C. Xu, *Fuel*, 117 (2014) 470-477.
- [49] L.P. Ozorio, R. Pianzolli, M.B.S. Mota, C.J. Mota, *J. Braz.Chem. Soc.*, 23 (2012) 931-937.

FIGURE CAPTIONS

Figure 1: XRD patterns of Niobic acid, 1Nb:1Al, 1Nb:0.6Al, 1Nb:0.3Al, 1Nb:0.1Al, 1Nb:0.05Al and Nb₂O₅.

Figure 2: FTIR spectra of 1Nb:1Al, 1Nb:0.6Al, 1Nb:0.3Al, 1Nb:0.1Al, 1Nb:0.05Al, Niobic acid; Nb₂O₅.

Figure 3: Raman spectra of (a) 1Nb:1Al, 1Nb:0.6Al and Niobic acid; (b) 1Nb:0.3Al, 1Nb:0.1Al, 1Nb:0.05Al and Nb₂O₅.

Figure 4: Infrared spectrum of chemisorbed pyridine over γ -Al₂O₃, 1Nb:1Al, 1Nb:0.6Al and 1Nb:0.3Al at 423 K.

Figure 5: N₂ adsorption/desorption isotherms of (a) 1Nb:1Al, 1Nb:0.6Al and (b) 1Nb:0.3Al, 1Nb:0.1Al, 1Nb:0.05Al.

Figure 6: Pore distribution of (a) 1Nb:1Al, 1Nb:0.6Al and (b) 1Nb:0.3Al, 1Nb:0.1Al, 1Nb:0.05Al.

Figure 7: Thermogravimetric analysis of 1Nb:1Al, 1Nb:0.6Al, 1Nb:0.3Al, 1Nb:0.1Al and 1Nb:0.05Al.

Figure 8: Differential thermal analysis of 1Nb:1Al, 1Nb:0.6Al, 1Nb:0.3Al, 1Nb:0.1Al and 1Nb:0.05Al.

Figure 9: Effect of the variation of the glycerol to acetone ratio on the acetalization reaction (2.7 wt% of catalyst, 6 h at 323 K): (a) glycerol conversion and (b) solketal selectivity.

Figure 10: Thermogravimetric analysis of the calcined 1Nb:1Al, 1Nb:0.6Al, 1Nb:0.3Al, 1Nb:0.1Al and 1Nb:0.05Al.

Figure 11: Kinetic study (solid lines) and leaching test (dashed lines) of the acetalization of acetone with glycerol catalyzed by 1Nb:1Al, 1Nb:0.6Al, 1Nb:0.3Al, 1Nb:0.1Al and 1Nb:0.05Al (glycerol:acetone molar ratio of 1:4, 2.7 wt% of catalyst, 323K).

Figure 12: Solketal and 6MR selectivity in function of time of the acetalization of glycerol with acetone catalyzed by 1Nb:1Al, 1Nb:0.6Al, 1Nb:0.3Al, 1Nb:0.1Al and 1Nb:0.05Al (glycerol:acetone molar ratio of 1:4, 2.7 wt% of catalyst, 323K).

Figure 13: Recycling tests of the 1Nb:1Al at 353 K, 1Nb:0.3Al and 1Nb:0.1Al at 323K in the acetalization of glycerol with acetone (glycerol:acetone molar ratio of 1 : 4, 2.7 wt% of catalyst, 6 h).

Scheme 1: Acetalization of acetone with glycerol.

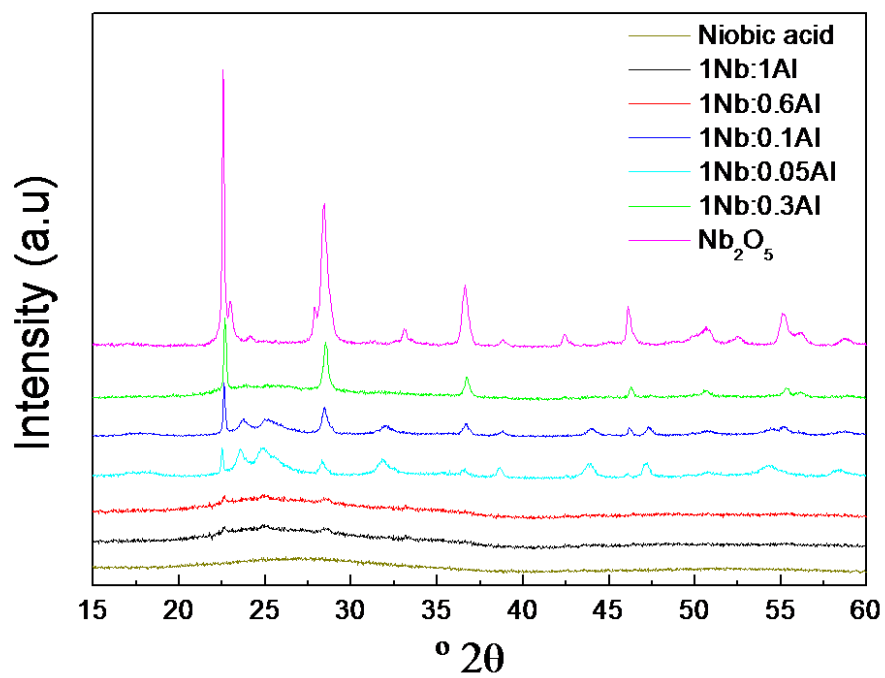


Fig. 1

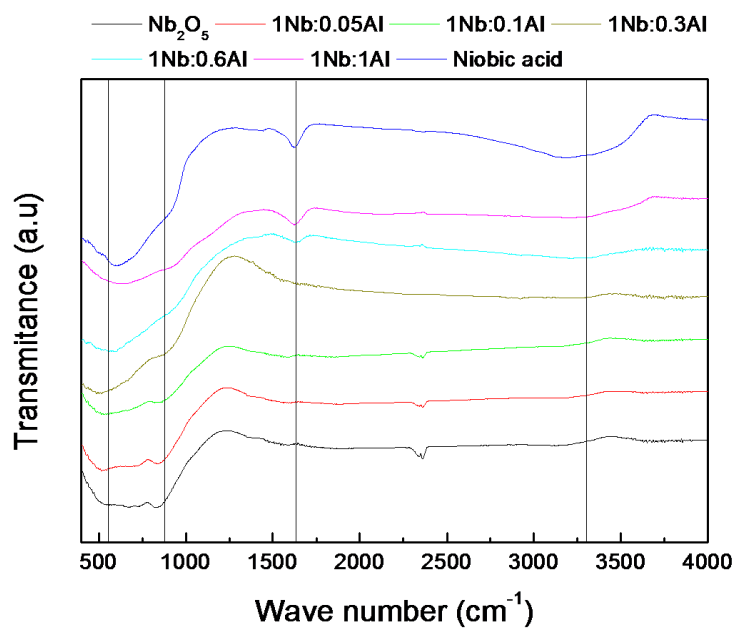


Fig. 2

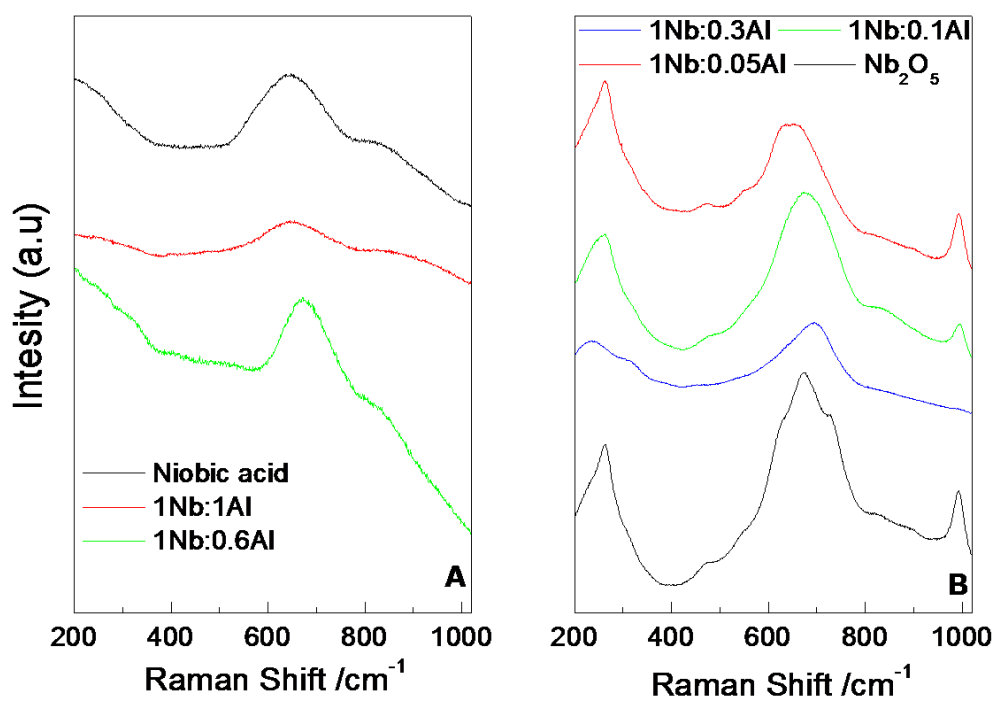


Fig. 3

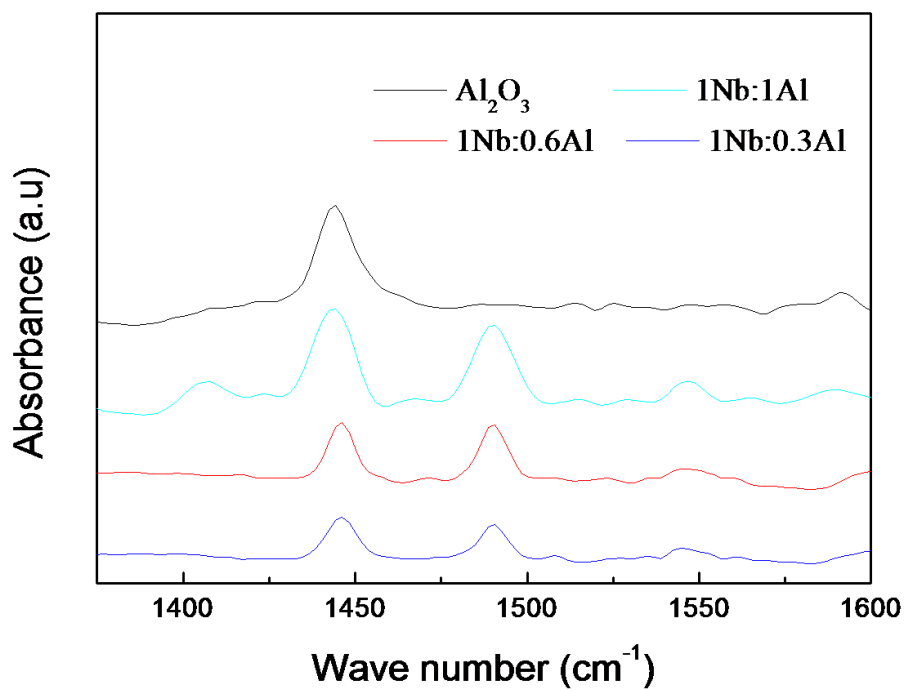


Fig. 4

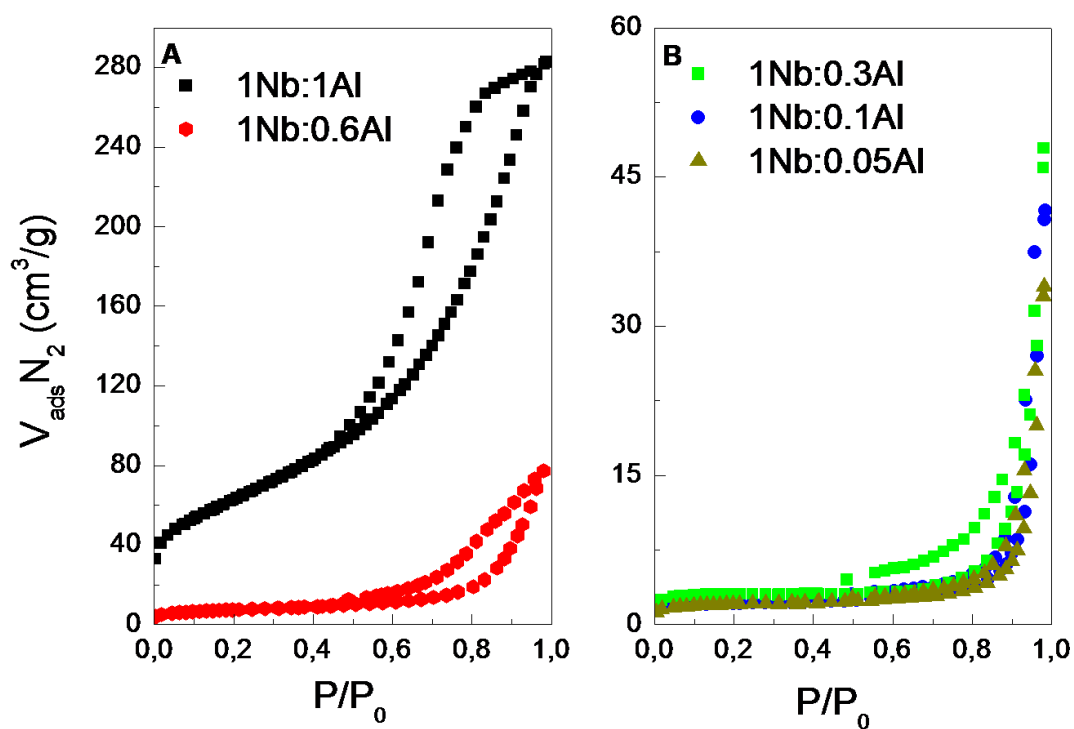


Fig. 5

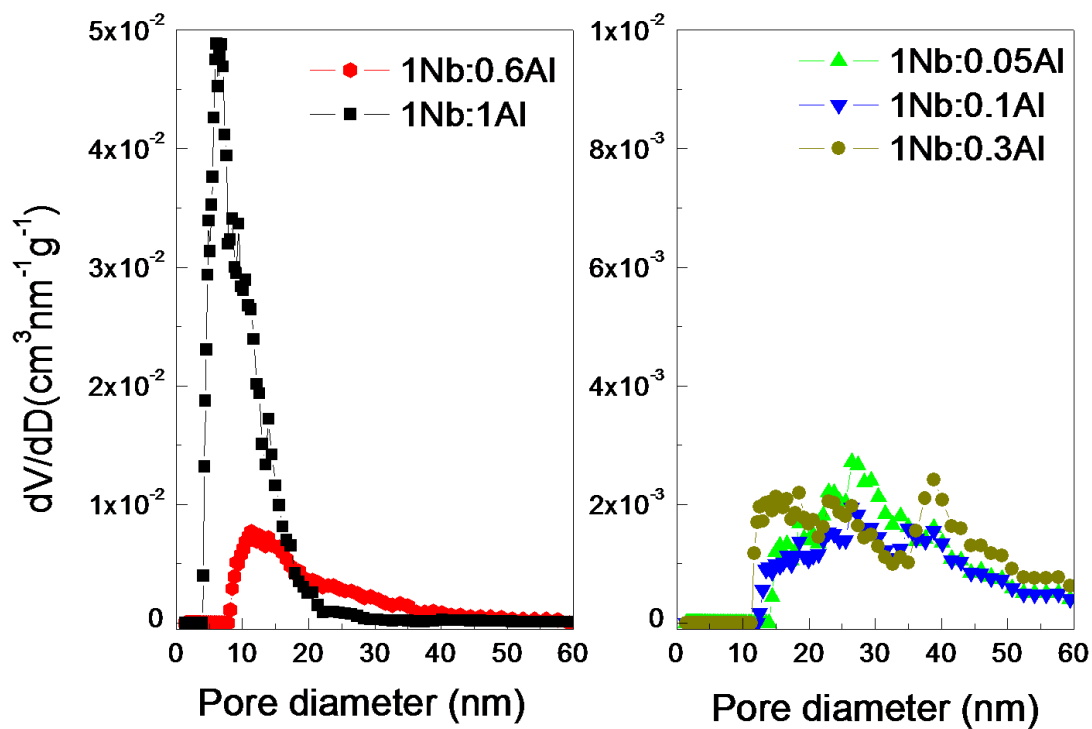


Fig. 6

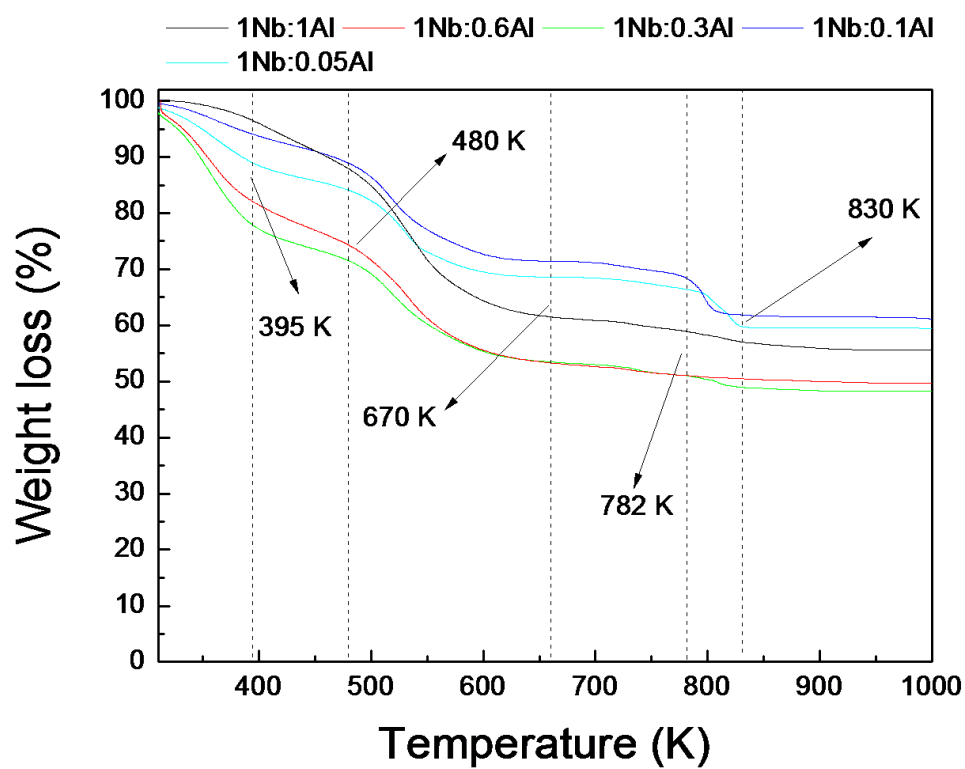


Fig. 7

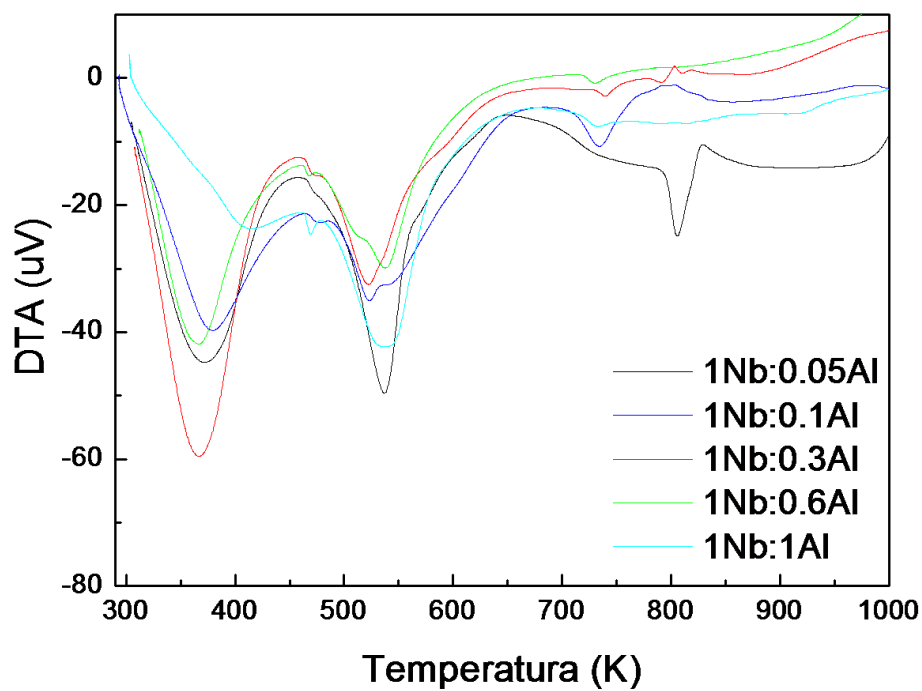


Fig. 8

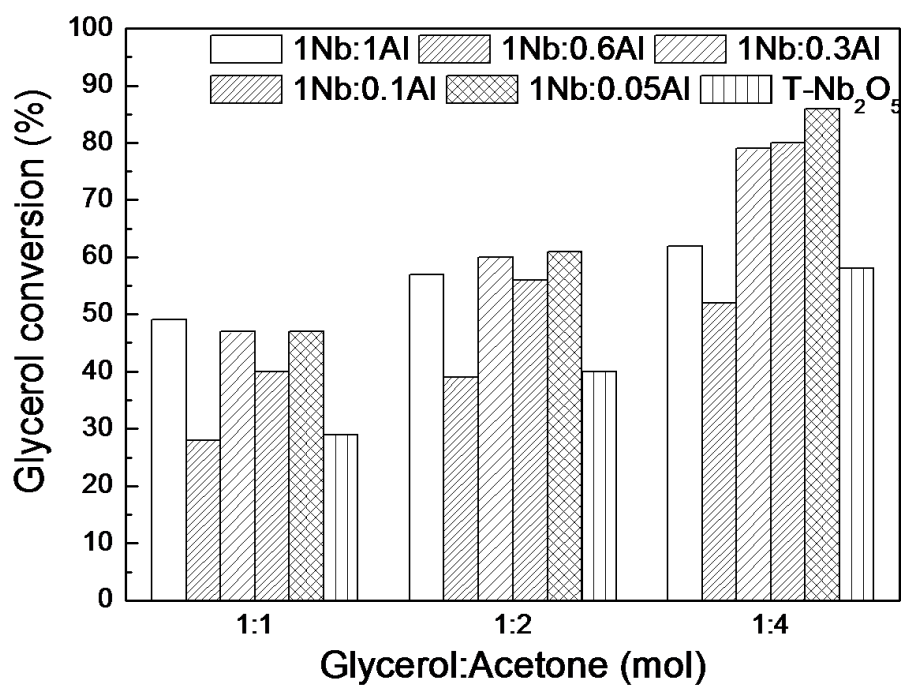


Fig. 9a

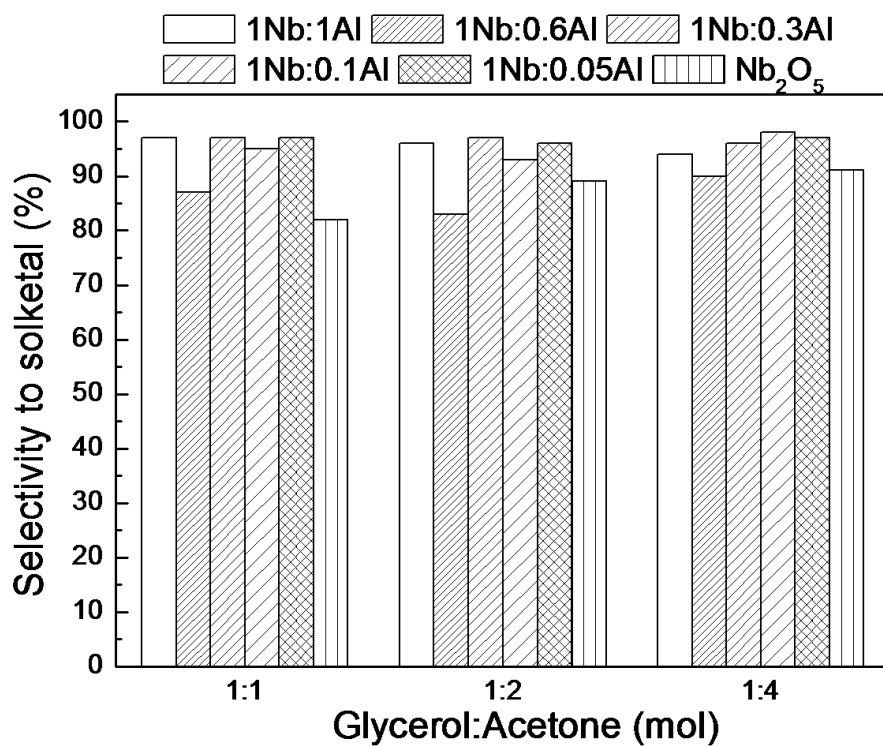


Fig. 9b

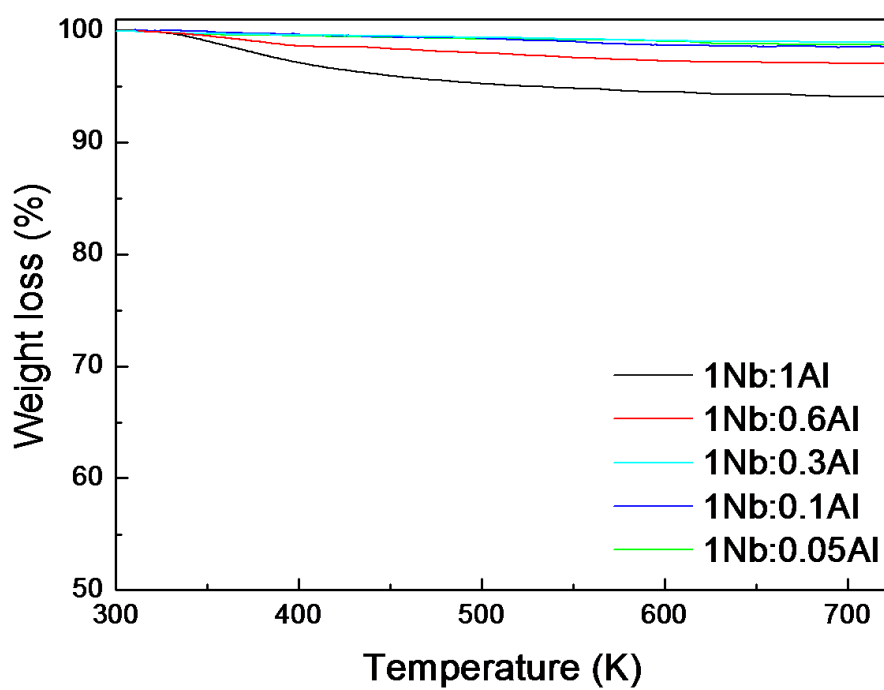


Fig. 10

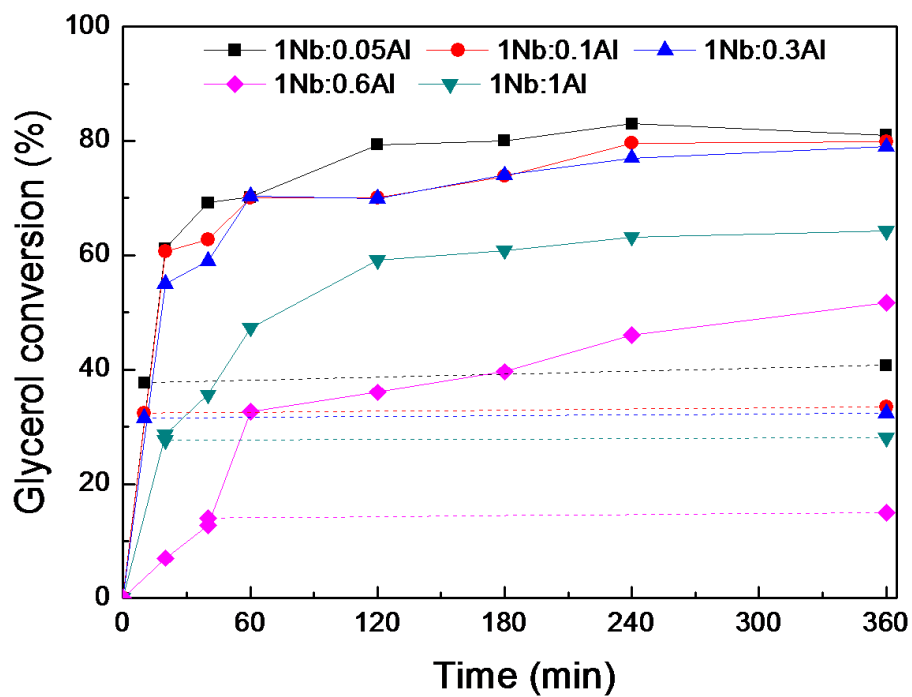


Fig. 11

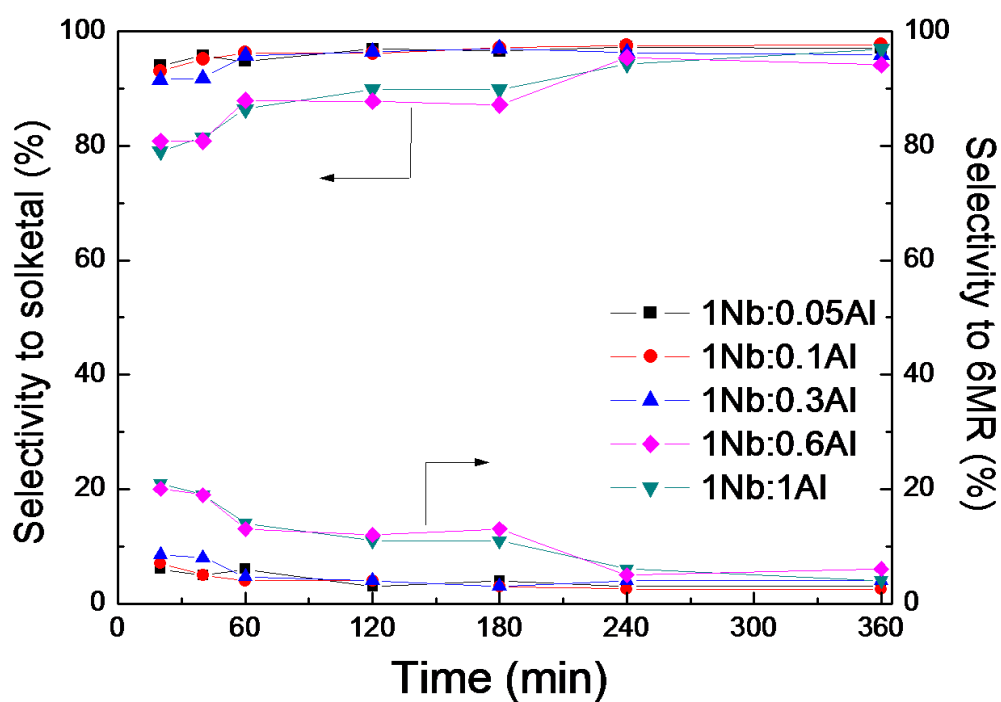


Fig. 12

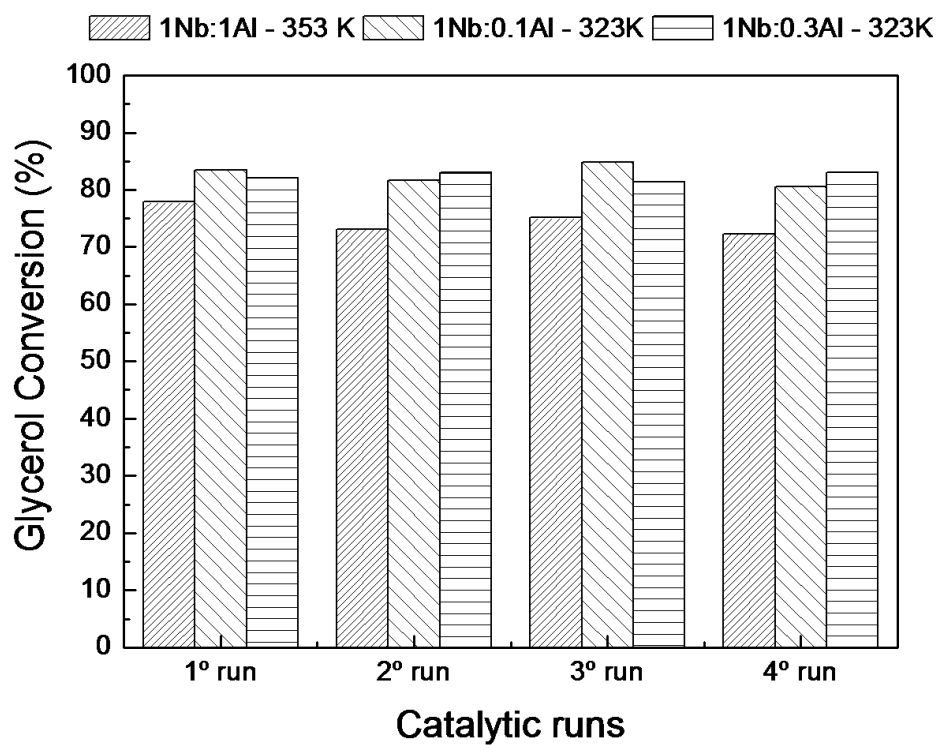
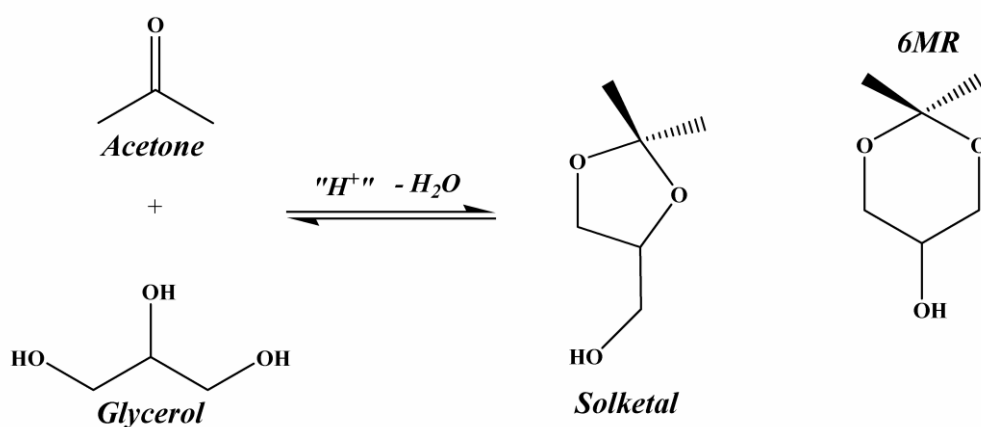


Fig. 13



Scheme. 1

Table 1: Textural properties and acidity of 1Nb:1Al, 1Nb:0.6Al, 1Nb:0.3Al, 1Nb:0.1Al and 1Nb:0.05Al.

Catalysts	Surface area (m ² g ⁻¹)	Total pore volume (cm ³ g ⁻¹)	Total acid sites ^{*a} (mol kg ⁻¹)	Lewis acid sites ^{*b} (mol kg ⁻¹)	Brønsted acid sites ^{*b} (mol kg ⁻¹)
1Nb:1Al	182	0.35	0.65	0.43	0.031
1Nb:0.6Al	36	0.12	0.12	0.10	0.012
1Nb:0.3Al	14	0.07	0.10	0.09	0.008
1Nb:0.1Al	<10	0.05	0.089	n.d	n.d
1Nb:0.05Al	<10	0.06	0.094	n.d	n.d

*Thermal desorption of pyridine monitored by (a) TGA and (b) FT-IR spectroscopy;

n.d = not detected.

Table 2: Acetalization of acetone with glycerol over 1Nb:1Al, 1Nb:0.6Al, 1Nb:0.3Al, 1Nb:0.1Al and 1Nb:0.05 Al at room temperature, 323 and 353 K (glycerol:acetone molar ratio of 1:4, 2.7 wt% of catalyst, 6 h).

	Glycerol conversion (%)	Selectivity to solketal (%)	Selectivity to 6MR (%)	Temperature (K)
1Nb:1Al	36	80	20	298
1Nb:0.6Al	26	75	25	
1Nb:0.3Al	69	95	5	
1Nb:0.1Al	66	93	7	
1Nb:0.05Al	73	93	7	
1Nb:1Al	62	94	6	323
1Nb:0.6Al	52	90	10	
1Nb:0.3Al	82	97	3	
1Nb:0.1Al	83	98	2	
1Nb:0.05Al	84	98	2	
1Nb:1Al	78	97	3	353
1Nb:0.6Al	69	97	3	
1Nb:0.3Al	75	97	3	
1Nb:0.1Al	77	97	3	
1Nb:0.05Al	77	97	3	